Charge Carrier Trapping and Acoustic Phonon Modes in Single CdTe Nanowires

Shun Shang Lo,[†] Todd A. Major,[†] Nattasamon Petchsang,[†] Libai Huang,[‡] Masaru K. Kuno,[†] and Gregory V. Hartland[†,*]

[†]Department of Chemistry and Biochemistry and [‡]Notre Dame Radiation Laboratory, University of Notre Dame, Notre Dame, Indiana 46556-5670, United States

ABSTRACT Semiconductor nanostructures produced by wet chemical synthesis are extremely heterogeneous, which makes single particle techniques a useful way to interrogate their properties. In this paper the ultrafast dynamics of single CdTe nanowires are studied by transient absorption microscopy. The wires have lengths of several micrometers and lateral dimensions on the order of 30 nm. The transient absorption traces show very fast decays, which are assigned to charge carrier trapping into surface defects. The time constants vary for different wires due to differences in the energetics and/or density of surface trap sites. Measurements performed at the band edge compared to the near-IR give slightly different time constants, implying that the dynamics for electron and hole trapping are different. The rate of charge carrier trapping was observed to slow down at high carrier densities, which was attributed to trap-state filling. Modulations due to the fundamental and first overtone of the acoustic breathing mode were also observed in the transient absorption traces. The quality factors for these modes were similar to those measured for metal nanostructures, and indicate a complex interaction with the environment.

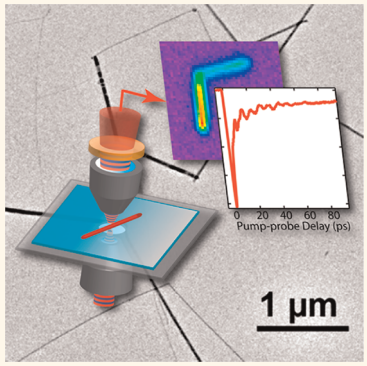

KEYWORDS: transient absorption microscopy · semiconductor nanowires · acoustic phonon modes · charge carrier trapping

Semiconductor nanowires (NWs) are promising materials for a variety of applications, such as solar cells,[1] lasers,[2] logic gates,[3] and transport of charge carriers.[4] Despite the many examples of NW-based devices and improved synthetic methods allowing the production of high quality structures, the fundamental processes occurring in these materials, such as exciton dephasing, are little understood. Studies of ultrafast dynamics in NWs are few, and have mainly been confined to a limited number of materials,[5] such as ZnO and cadmium chalcogenides.[6−9] The majority of the ultrafast studies of semiconductor nanostructures have been ensemble measurements,[5] that yield average rate constants for charge carrier relaxation. These experiments show that effects such as surface chemistry and composition can cause large changes in the charge carrier dynamics.[5] In this paper we use transient absorption microscopy to study the ultrafast dynamics of single CdTe NWs.[10] The results show a broad distribution of charge carrier trapping times, and that the dynamics are strongly influenced by trap-filling.[11,12] This unique information is made possible by the single particle experiments: details about how the dynamics vary within the ensemble cannot be obtained from conventional transient absorption measurements.

Coherently excited acoustic phonon modes are also observed in our measurements, which are assigned to breathing modes of the NWs. In semiconductors, interaction between excitons and acoustic phonons, either by direct coupling or through scattering processes, is one of the main contributions to the dephasing of the exciton resonance.[13−16] These vibrational modes also play an important role in carrier mobility[17] and the Stokes shift.[18] Acoustic phonon modes have been investigated in colloidal quantum dots (QD) using frequency-domain photoluminescence and Raman measurements,[19−22] and time-domain techniques,[23−28] and the spectral amplitudes provide data about the coupling to excitons.[15] However, information about the lifetimes of the acoustic phonon modes is difficult to obtain in ensemble measurements, as the damping is dominated by inhomogeneity in the size distribution.[29] Our measurements are the first observation of coherently excited phonon modes in single semiconductor nanostructures, and the measured decay times give fundamental information about energy relaxation in these materials.

RESULTS AND DISCUSSION

Selection of Single Nanowires. The ensemble linear absorption and transient absorption (TA) spectra, at 0 ps pump−probe delay, for our CdTe NW sample are presented in Figure 1a. CdTe was chosen for these studies because the

* Address correspondence to ghartlan@nd.edu.

Received for review March 9, 2012 and accepted May 4, 2012.

Published online May 04, 2012
10.1021/nn3010526

band edge is within the tuning range of the laser system used in the single particle TA experiments. The two prominent features observed in the TA spectra, a bleach at ~750 nm and an induced absorption at ~810 nm, are labeled as B1 and A1, respectively, following the nomenclature used in previous works.[30−37] Similar to CdSe QDs[30,31] and NWs,[8] and CdTe QDs,[32] the B1 feature is assigned to bleaching of the lowest optical absorption transition from state filling.[33−36] The A1 feature arises from red shifting of the lowest absorption feature due to the presence of charge carriers created by the pump pulse (either free or trapped carriers).[34−36] Note that transitions from trap states to the conduction band are also possible, but typically occur much further into the near-IR.[36,37] For QDs there has been extensive work to determine the relative contributions from electrons and holes to these features.[30−37] The general consensus is that the B1 feature primarily involves electron states,[33−35] whereas both electrons and holes can contribute to the near-IR absorption, with weights that depend on the wavelength.[35−37] The NWs used in our studies have relatively large diameters, and are outside the quantum confinement region.[32] The lack of exciton features makes it difficult to assign the near-IR absorption to specific transitions, and also means that a bulk-like description of the NW optical properties may be more appropriate.[16] In the single wire measurements discussed as follows, we focus on probing the time evolution of the A1 and B1 features.

Figure 1c shows high and low resolution transmission electron microscopy (TEM) images of the sample, which contains a large number of branched structures. The lengths of the nanowires vary from one to several micrometers, and the average width is 29 nm with a standard deviation of 10 nm (a histogram of the nanowire widths is given in the Supporting Information). The bands that can be seen in the high-resolution TEM images arise from twinning between the wurtzite and zinc-blende phases of CdTe.[38]

To ensure that a single wire is being measured in the transient absorption experiments, isolated branched structures are selected because they are unlikely to form bundles, as can be seen in the TEM images. The NWs were found by observing scattered light from the sample; a representative scattered light image of a branched CdTe nanowire is shown in Figure 2a. For all the experiments described in what follows, the samples were covered in microscope oil, which allows the nanostructures to be clearly seen in scattering. The nano-object in Figure 2a appears smooth in the image, and has a characteristic shape consistent with those in the TEM images. This nanostructure is, therefore, likely to be a single branched NW. For many of the nanowires interrogated in the ultrafast experiments, additional confirmation that the object is a single nanowire was obtained by measuring the

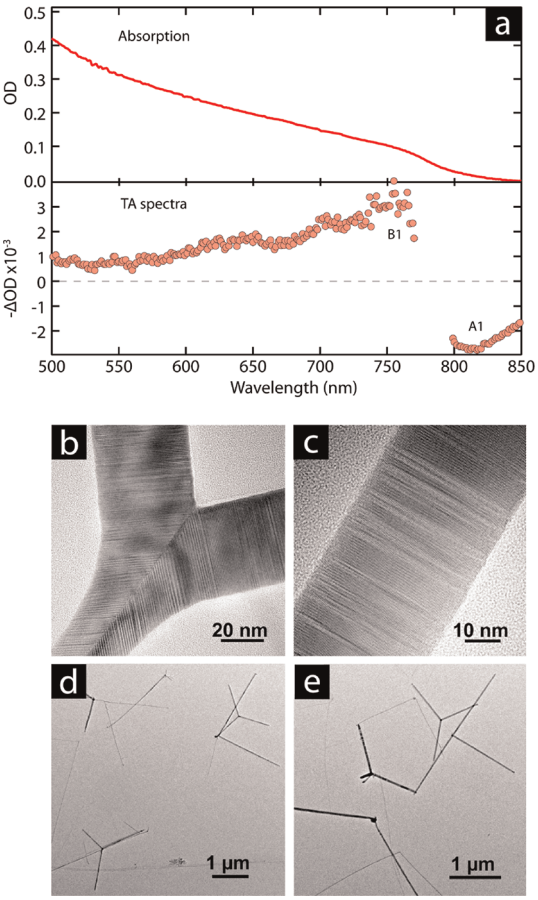

Figure 1. (a) Upper panel: Ensemble linear absorption spectra of the CdTe NW sample. Lower panel: Corresponding ensemble transient absorption spectra at 0 ps pump−probe delay time. Two prominent features are observed, a bleach (B1) at ~750 nm and an induced absorption (A1) at ~810 nm. (b−e) High and low resolution TEM images of representative CdTe NWs.

extinction cross-section. This gives an estimate of the NW radius, and allows single nanowires to be differentiated from bundles.

Extinction cross-section measurements were performed by moving the NW in-and-out of the beam path, in either the *x* or the *y* direction, using a piezoelectric stage.[39,40] As the wire crosses the laser focus, a drop in transmission is observed. Traces obtained in this way are shown in Figure 2b for each arm of the NW in Figure 2a (note the color coding). Each trace is an average over 10 scans and has been normalized to the background. The maximum percentage drop in transmission, $|\Delta P/P|$, is related to the extinction cross section, σ_{NW}, through[41]

$$\sigma_{NW} = \omega_0 \sqrt{\frac{\pi}{2}} \times \left| \frac{\Delta P}{P} \right| \quad (1)$$

where the Gaussian beam waist $\omega_0 = 0.42 \pm 0.01$ μm was determined in a separate measurement. Circularly polarized light was used in our optical measurements, which means that $\sigma_{NW} = (\sigma_{\parallel} + \sigma_{\perp})/2$. Values of σ_{NW} were calculated for different nanowire radii to

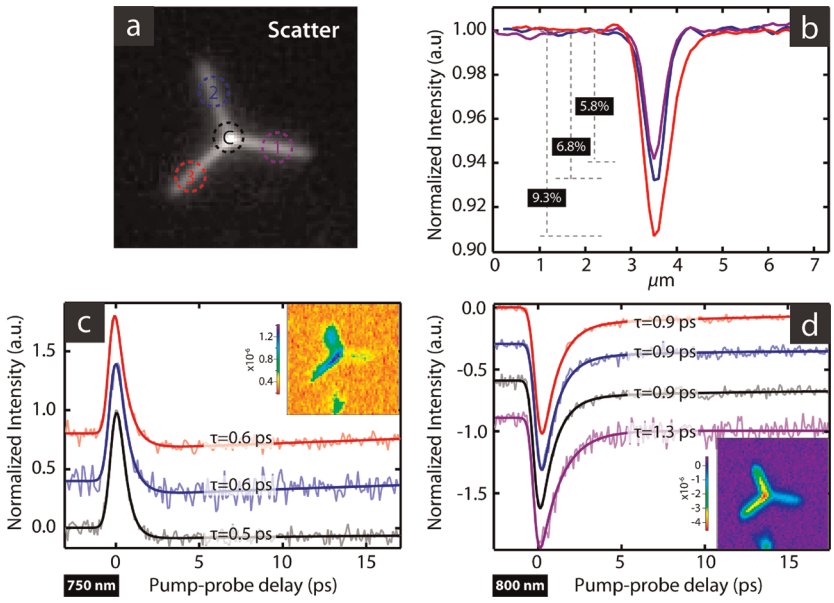

Figure 2. (a) Scattered light image of a typical branched CdTe wire used in this study. (b) Extinction measurements using the procedure described in text. The percentage drop in transmission is related to the extinction cross section σ_{NW} through eq 1. (c) Transient absorption traces at the B1 feature at different spatial points of the wire. The dominant time constant for each trace is shown in the figure, the error is estimated to be ±0.1 ps. Inset is the transient absorption image of the wire. (d) Same as panel c at the A1 feature. For panels b–d the color of the traces correspond to the positions marked by the dashed circles in panel a.

generate a calibration curve (see Supporting Information), using the absorption and scattering cross sections for an infinite cylinder given in ref 42. For the NW in Figure 2, comparison between the calculations and experimental measurements gave values of the radii of 13.2 ± 0.3 nm (arm 1, purple trace), 14.4 ± 0.2 nm (arm 2, blue trace) and 17.4 ± 0.5 nm (arm 3, red trace). These sizes are consistent with the TEM images of NWs with similar morphologies; therefore, this nanostructure is likely to be a single wire and appropriate for use in subsequent TA measurements.

Charge Carrier Relaxation. Once a wire has passed the selection process described above, transient absorption images at fixed pump–probe delay times, and transient absorption traces at different spatial positions within the wire were recorded. The TA images and decays corresponding to the branched wire shown in Figure 2a are presented in Figure 2c,d for probe wavelengths of 750 nm (at the B1 bleach feature) and 800 nm (at the A1 induced absorption feature). The wavelengths of the pump pulse were 375 and 400 nm, respectively, and the pump intensity was set to 0.4 pJ/pulse before the microscope for these experiments. The TA images at the B1 feature show spatial variations in the signal intensity. Qualitatively, the signal is strongest at the thickest arm while it is weakest at the thinnest arm. This is expected since the transient absorption and bleach signals are proportional to the absorption cross-section of the nanostructure. The TA image at the A1 feature shows similar spatial trends in signal intensity. The signal levels are worse when probing at 750 nm compared to 800 nm because the efficiency of the optical components in our microscope is decreased at wavelengths <400 nm, which means that the pump beam is attenuated at the sample in the former experiments.

The time-resolved traces at both the A1 and B1 features are dominated by a fast decay, on the order of a picosecond, followed by a weaker long time absorption signal. Fits to the traces with a single exponential convoluted with the instrument response function, plus a slower absorption signal are shown as solid lines in Figure 2c,d. The time constants for the exponential decays extracted from these fits are given in the figure. The colors for the traces correspond to the spatial positions marked by circles of the same color in Figure 2a. The time constants for the A1 and B1 decays are similar, with the A1 feature decaying on a slightly longer time scale for the NW in Figure 2. The time scale for these decays are consistent with those found in previous ensemble and single NW studies for CdTe.[9,10]

Several possible processes could be responsible for the fast decay observed in the transient absorption traces: diffusion of charge carriers out of the probe region,[43,44] carrier thermalization *via* electron–phonon coupling and/or Auger processes,[30,31] charge carrier trapping,[5,32] or Auger recombination.[30] The decay times observed are too fast to correspond to charge carrier diffusion: we estimate that diffusion out of the probe region should occur on a tens of picoseconds times scale from the electron mobility in bulk CdTe.[45] To confirm that diffusion is not important, measurements were also performed on single CdSe nanowires (see Supporting Information). The decay

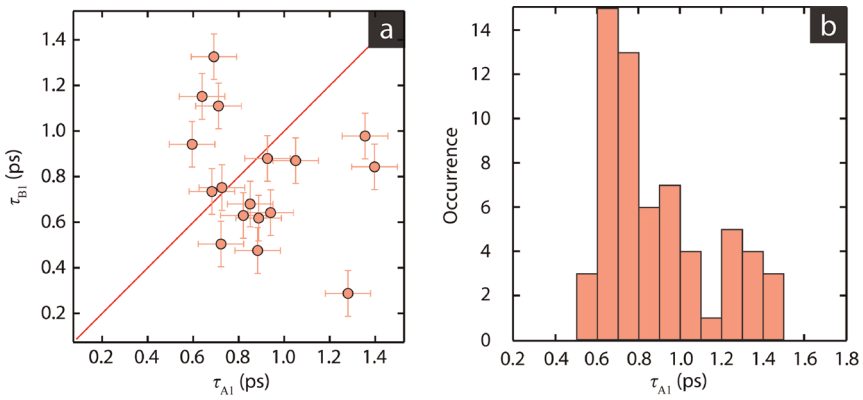

Figure 3. (a) A scatter plot of the dominant time constant at the B1 feature *versus* that at A1. (b) Histogram of τ_{A1}, the dominant time constant of the decay at the A1 feature.

times are much longer, on the order of 30−50 ps. Given that the charge carrier mobilities are similar for CdTe and CdSe,[45] these results show that charge carrier diffusion is not significant on the picosecond time scale of our measurements. The comparison between CdTe and CdSe also implies that the measured dynamics are not due to carrier thermalization. In bulk semiconductors excited charge carriers lose energy by emission of optical phonons, with a typical rate of 0.5 eV/ps,[30] which is similar for CdTe and CdSe.[46] For our experiments this would correspond to a few ps timescale process. This process could, in principle, appear in the transient absorption traces. However, it should be present for both CdSe and CdTe.

The decays in the transient absorption traces could also arise from electron−hole recombination through Auger processes,[30,31] or mediated by trap sites. Trap mediated recombination is usually a much longer time scale process in semiconductor nanostructures,[5] and can be discounted. The rate of Auger recombination can be estimated from the Auger rate constants reported in ref 8 for CdSe NWs. For the carrier densities used in our experiments (see below), we estimate an Auger recombination time of *ca.* 40 ps. This is much slower than the fast time scale decays seen in Figure 2.

On the basis of the above considerations, the short time dynamics observed in the transient absorption traces for CdTe are assigned to charge carrier trapping into surface states.[10,32] Trapping produces a change in the A1 signal because free carriers and trapped carriers have different optical absorption cross sections. The background absorption signal that is present in all the transient absorption traces shows that the charge carriers remain trapped for relatively long times. The assignment of the dynamics to charge carrier trapping is consistent with the low quantum yields for these CdTe NWs.[38] Note that the fast time constants in our experiments are the same order of magnitude as the 1.7 ps hole trapping time measured for CdTe QDs.[32] The difference between our measurements and those in ref 32 most likely arises from differences in the surface chemistry of the samples. The fast trapping times for the CdTe NWs also implies that there could be significant trapping of hot carriers in this system.[47,48]

Performing measurements at the single particle level allows several issues to be examined that cannot be accessed in conventional ensemble measurements. For example, Figure 3a shows a scatter plot of the time constants measured at the B1 (τ_{B1}) and A1 (τ_{A1}) features. Each point in this plot corresponds to a different NW, with the two experiments being performed at the same spatial position in the NW. The data in Figure 3a shows that τ_{B1} and τ_{A1} are similar in magnitude but, in general, have different values. There is very little correlation between the two time constants—the correlation coefficient for the data in Figure 3a is −0.28, which implies uncorrelated measurements.[49] These experiments were performed at low pump fluence ≤0.13 mJ/cm^2, corresponding to <0.13 electron−hole pairs per nm^3. This is well below the level where intensity dependent effects are observed (see below). The differences in the B1 and A1 decay times imply that experiments at these two features monitor different processes. On the basis of the QD literature, we propose that experiments at B1 primarily probe electron dynamics, whereas, experiments at A1 have contributions from both electrons and holes.[30−37] The observation that for some NWs $\tau_{A1} > \tau_{B1}$, while for others $\tau_{A1} < \tau_{B1}$, implies uncorrelated variations in the trapping times for the electrons and holes.

Figure 3b shows a histogram of the τ_{A1} values recorded for 61 NWs (the experiments are easier to perform at the A1 feature, thus we have concentrated on this feature to generate statistics for the charge carrier trapping process). Most wires have values of $\tau_{A1} < 1$ ps, but a significant fraction have $\tau_{A1} > 1.2$ ps. The average value of τ_{A1} is 0.9 ps, with a standard deviation of 34%. The wide distribution of trapping times observed for our measurements on CdTe is similar to a recent report for ZnO nanostructures.[50] These results imply that there are significant variations

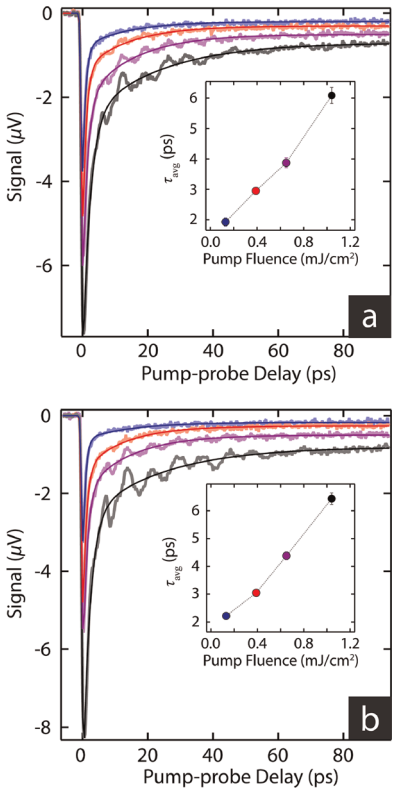

Figure 4. (a and b) Decay of the A1 feature as a function of pump fluence for two representative CdTe nanowires. The *y*-axis gives the root-mean-square signal recorded by the lock-in amplifier. The insets show the amplitude weighted average lifetimes for the two NWs in panels a and b. The colors of the data points in the insets correspond to the colors of the transient absorption traces.

in the energy and/or density of the electron and hole trap states in the NWs, presumably because of variations in the surface chemistry, that cause differences in the trapping times.[3,10] No correlation was observed between the trapping times and the radius of the NWs.

Figure 4 panels a and b present decays recorded at the A1 feature for two representative wires as a function of pump fluence. As the excitation intensity increases the time scale for charge carrier trapping becomes longer, and there is an increase in the background induced absorption signal. The increase in the background absorption is also seen in the 750 nm probe experiments (see the Supporting Information). The traces in Figure 4a and b were fit to a biexponential function plus an offset, convoluted with the instrument response function. The amplitude weighted average time constants $\tau_{avg} = (a_1\tau_1 + a_2\tau_2)/(a_1 + a_2)$, where a_1 and τ_1 and a_2 and τ_2 are the weights and time constants for the two exponentials, respectively, are plotted *versus* fluence in the insets of Figure 4a,b. Note that in almost all studies of semiconductor nanostructures, an increase in excitation intensity produces a fast decay component, which can be due to either Auger recombination,[30,31,51] or dynamics associated with forming an electron–hole plasma.[7,52] Thus, the

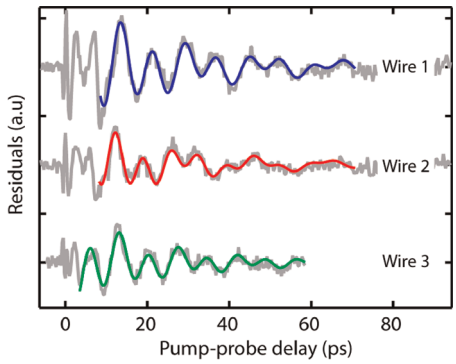

Figure 5. Acoustic phonon modes of representative CdTe nanowires. Gray traces are residuals from the decay fits (see Figure 4); colored lines are fits to the residuals using a damped-double cosine function. The periods and damping times are given in Table 1.

intensity dependent results in Figure 4 are somewhat unusual.

Charge carrier trapping is a second order process that depends on the number of free charge carriers and the number of empty trap states.[11,12,16] As the pump fluence increases, the trap states fill up, which reduces the rate of trapping. The intensity-dependent results in Figure 4 are thus a clear signature of trap state filling in semiconductor NWs.[11,12] The trap filling mechanism is consistent with the increase in the background signal for the A1 feature at high pump intensities. Trap state filling has been previously invoked to explain fluorescence quantum yield measurements for semiconductor nanowires[11,12] and QDs,[53] but to the best of our knowledge it has not been directly observed in time-resolved measurements for these materials until now.

Acoustic Phonon Modes. Ultrafast excitation of semiconductor nanostructures can also coherently excite phonon modes of the material. Modulations can be clearly seen in the data recorded at high pump fluence in Figure 4. Figure 5 shows the oscillating component of the data, obtained by subtracting a biexponential function plus a background from the transient absorption traces (see Figure 4). The solid lines in Figure 5 represent a fit to the data using a damped double cosine function. The periods extracted for the oscillations are ~7 and ~16 ps, and are the same order of magnitude as those expected for the acoustic phonon modes. While there are abundant reports on the observation of acoustic phonons in colloidal semiconductor quantum dots,[23–28] there are no reports of these modes for solution-based NWs to date. Similar to CdSe QDs, both the frequency and phase of the oscillations are independent of the pump intensity, indicating that within the pump fluence range employed in the measurements the elastic properties of the wires have not been modified.[24] The amplitudes of the oscillation were found to increase as a function of increasing pump intensity (see Supporting Information), as is the case for CdSe QDs.[24]

TABLE 1. Periods and Damping Times for the Acoustic Phonon Modes[a]

	wire 1	wire 2	wire 3
radius (nm)	18.5 ± 0.4	15.8 ± 0.2	14.1 ± 0.4
$T_{br}^{(0)}$ (ps) expt	17.6 ± 0.2	17.6 ± 0.2	15.5 ± 0.3
$T_{br}^{(0)}$ (ps) theory	16.4	14.0	12.5
$T_{br}^{(1)}$ (ps) expt	7.8 ± 0.1	6.7 ± 0.1	7.2 ± 0.1
$T_{br}^{(1)}$ (ps) theory	6.6	5.6	5.0
$\tau_{damp}^{(0)}$ (ps)	59.8 ± 17	53.3 ± 11	24.4 ± 4
$\tau_{damp}^{(1)}$ (ps)	23.8 ± 1.7	17.9 ± 1.5	22.4 ± 1.9
$Q^{(0)}$	10.7 ± 3.2	9.5 ± 2.1	5.0 ± 0.9
$Q^{(1)}$	9.6 ± 0.8	8.4 ± 0.8	9.8 ± 1.0
$A^{(1)}/A^{(0)}$	2.0	1.0	2.0

[a] The radii of the wires were estimated from the extinction cross-section measurements. $T_{br}^{(n)}$ is the period of the nth breathing mode, $\tau_{damp}^{(n)}$ is the damping time, $Q^{(n)}$ is the corresponding quality factor, and $A^{(1)}/A^{(0)}$ is the relative amplitude of the $n = 0$ and $n = 1$ modes. The calculated periods were obtained from the measured radii using eq 3 and 4 in the text.

In experiments on 1D nanostructures, ultrafast laser excitation coherently excites the extension and breathing modes.[54] Modeling the NWs as long, elastically isotropic cylinders yields the following expressions for the extensional and breathing mode frequencies:[54]

$$\omega_{ext}^{(n)} = \frac{2n+1}{L}\pi\sqrt{\frac{E}{\rho}} \quad (2)$$

$$\omega_{br}^{(n)} = \frac{\xi_n}{a}c_L \quad (3)$$

where $n = 0, 1, 2, \ldots$ is the mode number, E is Young's modulus, ρ is the density, c_L is the longitudinal speed of sound, a is the radius of the cylinder, and L is its length. The eigenvalue ξ_n for the breathing mode is obtained from the roots of the equation

$$\xi_n J_0(\xi_n) = \frac{1-2\nu}{1-\nu}J_1(\xi_n) \quad (4)$$

where ν is Poisson's ratio and $J_m(\xi)$ are Bessel functions of order m. For CdTe, $E = 38.2$ GPa, $\rho = 5854$ kg/m^3, $c_L = 3234$ m/s, and $\nu = 0.35$.[55]

The typical lengths of the NWs used in this study are ≥ 1 μm. According to eq 2, the lowest frequency extension modes, which are predominantly excited in transient absorption experiments,[54] are expected to have periods on the nanosecond time-scale. This is much longer then the time-window of the current experiment, which means the oscillations in Figure 5 cannot be attributed to the extension modes. On the other hand, the predicted periods for the breathing modes are very similar to the experimental values, see Table 1. In this table the experimental values are compared to the values calculated through eq 3, with radii determined from the extinction cross-section measurements. The largest discrepancy between the calculated and measured periods is ~30%, which is reasonable considering that both the optical and the elastic constants of CdTe are not precisely known. Thus, the oscillations in the transient absorption traces are assigned to the breathing modes of the NWs.

It is interesting to note that both fundamental ($n = 0$) and overtone ($n = 1$) breathing modes are observed, with the latter having a slightly larger amplitude. The relative amplitudes of the $n = 0$ and $n = 1$ modes are included in Table 1. Higher order breathing modes have been observed in metal nanoparticles,[56] although the amplitude of the $n = 0$ mode is usually larger than that of the $n = 1$ mode. The $n = 1$ spheroidal mode has been observed in Raman experiments on ZnO nanoparticles,[57] but the selection rules for Raman are different to those in time-resolved measurements.[58] The amplitude of the acoustic breathing modes depends on both the excitation and probe processes. In our experiments the increased amplitude of the overtone compared to the fundamental most likely arises from how these modes couple to the probe transition. Calculations of the expected amplitudes are difficult, because of the complicated nature of the probe transition in these experiments, and we have not attempted this for this manuscript.

The damping time of the oscillations, $\tau_{damp}^{(n)}$, can also be extracted from the fits, allowing the calculation of the quality factor $Q^{(n)} = \pi\tau_{damp}^{(n)}/T_{br}^{(n)}$ for each phonon mode ($n = 0$ and 1); these are summarized in Table 1. Note that since the oscillations were observed at the single wire level, the extracted $\tau_{damp}^{(n)}$ values reflect the homogeneous damping time of the acoustic phonon modes. The Q values for the CdTe NWs are similar to those reported in single particle measurements on metal nanoparticles and NWs,[29,59,60] and ensemble experiments on highly monodisperse NP samples.[61] Typically values of $Q = 10$ are found for Ag, and $Q = 30-40$ for Au.[29,59,60]

The damping of the acoustic modes arises from radiation of sound waves into the surrounding medium.[62,63] Previous single particle results for metal nanostructures have been interpreted in terms of the miss-match between the acoustic impedance $Z = \rho.c_L$ of the particle and the surroundings.[29,59,63,64] Specifically, a large difference in Z causes reflection of sound waves at the interface, and long vibrational lifetimes. In contrast, for a small difference in Z, sound waves are transmitted through the interface, giving short vibrational lifetimes.[29,63] The acoustic impedance of CdTe ($Z = 18.9 \times 10^6$ kg m^{-2} s^{-1}) is much smaller than that of Au ($Z = 62.5 \times 10^6$ kg m^{-2} s^{-1}) or Ag ($Z = 38.3 \times 10^6$ kg m^{-2} s^{-1}), and is closer to the acoustic impedance of the environment. Thus, by the acoustic impedance miss-match model the quality factors for the acoustic vibrational modes should be smaller for CdTe compared to metal nanoparticles.

Our experiments with Ag nanowires showed that the damping of the breathing mode can be estimated by a formula derived for spherical particles

in a homogeneous medium.[29,59] The NWs in the present experiments are on a glass surface surrounded by microscope oil. For particles in a glass environment (ρ = 2240 kg/m^3, c_L = 5100 m/s, and c_T = 2840 m/s) the calculated quality factors for the fundamental and overtone breathing modes are $Q^{(0)}$ = 2.6 and $Q^{(1)}$ = 4.6, respectively, slightly smaller than the experimental values. This indicates incomplete contact with the glass substrate, and a possible role of the surrounding fluid in the damping of the vibrational modes.[65]

The acoustic mode damping calculations can be extended to include viscosity by writing the speeds of sound in the environment as $c_L = ((\lambda_L + 2\mu_L + i\omega(\lambda + 2\mu))/\rho)^{1/2}$ and $c_T = ((\mu_L + i\omega\mu)/\rho)^{1/2}$, where μ_L and λ_L are the Lame constants, and μ and λ are the shear viscosity and second viscosity coefficient.[66] This formalism was recently used to analyze results for single Au nanoparticles optically trapped in water.[67] The results showed a weak influence of solvent viscosity. However, the damping is strongly dependent on the frequency of the vibrational motion, and for the higher frequency modes in our experiments it becomes significant. For example, for water we calculate a quality factor of $Q^{(0)}$ = 12.5 for the fundamental breathing mode of the CdTe NWs, and $Q^{(1)}$ = 31.3 for the overtone. For viscous liquids the damping is even stronger; however, it is not clear that the theory is applicable to high frequency motions in viscous liquids.[61,66,67] These considerations show that the damping of the vibrational modes is probably influenced by both contact with the glass substrate, and the surrounding microscope oil. Experiments are currently being conducted on suspended nanowires to isolate the effect of fluids on vibrational damping.

CONCLUSIONS

Transient absorption measurements were conducted on single CdTe nanowires. At low excitation intensities (carrier densities of <0.13 nm^{-3}) decays at the bleach and induced absorption features were found to be fast, between 0.4 to 1.4 ps. This rapid decay is assigned to efficient charge carrier trapping. Examining multiple CdTe NWs revealed a large distribution of the decay times. This was attributed to inhomogeneity in the surface chemistry of the NWs used in these experiments, which causes different trapping times for the charge carriers in different NWs. When the excitation intensity was increased, the time scale for charge carrier trapping increased. This behavior is strikingly different to colloidal semiconductor QDs, where Auger processes cause faster kinetics at high pump powers,[30,31] and was attributed to trap-state filling.[11,12] At high pump intensities, oscillations were also observed in the transient absorption traces which were assigned to acoustic phonon modes, specifically, to the fundamental and overtone breathing modes of the NW.[56] The quality factors of these modes were on the order of $Q \approx 9-10$, which is similar to those observed in experiments on single metal nanostructures. These results represent the first time that acoustic phonon modes have been observed for semiconductor NWs, and are also the first observation of acoustic phonon modes in any single semiconductor nanostructure.

MATERIALS AND METHODS

CdTe nanowires were synthesized using a solution–liquid–solid growth method.[38,68] After synthesis, the wires went through several cleaning cycles using methanol and were then stored inside a glovebox to avoid oxidation.[69] The synthesized wires were found to have diameters of 29 ± 10 nm (error equals standard deviation), and lengths of several micrometers as measured under TEM. Samples for optical studies were prepared by drop casting onto a clean coverslip inside the glovebox. The sample was allowed to dry, then a drop of immersion oil was added and a second coverslip was placed on top; the edges of the coverslips were then sealed with nail polish. This sample preparation procedure greatly reduced the oxidation of the samples,[69] and allowed them to be studied for several days in the transient absorption microscopy experiments. The degree of oxidation was judged by observing the (weak) fluorescence from the sample: a decrease in fluorescence intensity implies sample oxidation.

Transient absorption measurements were performed using a Coherent Chameleon Ultra-II Ti:sapphire laser (repetition rate of 80 MHz). The output was sent through a Coherent 9200 pulse picker, set at 5 MHz, and then split by a 50/50 beam splitter. One of the beams was frequency doubled using a 0.5 mm BBO crystal (Castech) to produce the pump, while the second beam was used as the probe. The pump was chopped at 500 kHz using an acousto-optical modulator (Intra-Action Corp), triggered by a BK Precision 4011A function generator. The function generator was synchronized to the pulse-picker to ensure a consistent number of pump pulses per on–off cycle. A Newport UTM100PP.1 translation stage was used to control the relative delay between the pump and probe pulses. The instrument response function was estimated to be 0.3 ps, based on the rise time in transient absorption traces for materials with long excited state lifetimes. Quarter wave plates were used to set the polarizations of the pump and probe pulses to be circular, while their intensities were controlled by a half waveplate-polarizer combinations and neutral density filters.

The pump and probe beams were overlapped and focused onto the sample using an Olympus UPlan FLN100x 1.30 NA oil immersion objective. The transmitted beams were then recollimated using a matched objective. A long pass filter was employed to prevent any pump light from reaching the detector, and changes in the probe were monitored with an avalanche photodiode detector (Hamamatsu, C5331-03 or -11). The signal from the detector was measured with a RF-frequency lock-in amplifier (Stanford Research Systems, SR844) triggered by the function generator. Transient absorption images were recorded by raster scanning the sample with a piezoelectric stage (Physik Instrumente, P-527.3Cl). The piezo stage was also used for the extinction measurements in Figure 2b and Table 1. Ensemble transient absorption experiments were performed with a Clark-MXR CPA-2001 Ti:sapphire laser system, and an Ultrafast Systems transient absorption spectrometer.

The extinction cross sections for the nanowires were calculated using the expressions given in ref 42. These calculations were performed in Mathematica (version 8.01,

Wolfram Research, Inc.). The nanowire extinction cross sections were also estimated by Finite Element simulations using COMSOL Multiphysics (version 4.2a). The two calculations were in excellent agreement, validating the values used for the size analysis.

Conflict of Interest: The authors declare no competing financial interest.

Acknowledgment. This work was supported by the National Science Foundation through Award CHE-1110560 and CHE-0946447, and by the University of Notre Dame Strategic Research Initiative. L. Huang acknowledges the support from the Office of Basic Energy Science of the U.S. Department of the Energy (DE-FC02-04ER15533). The authors thank Prashant Kamat for use of his ultrafast laser system for the ensemble transient absorption experiments.

Supporting Information Available: Additional TEM images of the nanowire sample, a histogram of the width distribution, details of the extinction cross-section measurements, transient absorption results for single CdSe nanowires, and power-dependent transient absorption traces for the B1 feature. This material is available free of charge *via* the Internet at http://pubs.acs.org.

REFERENCES AND NOTES

1. Yu, Y.; Kamat, P. V.; Kuno, M. A CdSe Nanowire/Quantum Dot Hybrid Architecture for Improving Solar Cell Performance. *Adv. Funct. Mater.* **2010**, *20*, 1464–1472.
2. Duan, X.; Huang, Y.; Agarwal, R.; Lieber, C. Single-Nanowire Electrically Driven Lasers. *Nature* **2003**, *421*, 241–245.
3. Huang, Y.; Duan, X.; Cui, Y.; Lauhon, L.; Kim, K.; Lieber, C. Logic Gates and Computation from Assembled Nanowire Building Blocks. *Science* **2001**, *294*, 1313–1317.
4. Dorn, A.; Strasfeld, D. B.; Harris, D. K.; Han, H.-S.; Bawendi, M. G. Using Nanowires to Extract Excitons from a Nanocrystal Solid. *ACS Nano* **2011**, *5*, 9028–9033.
5. Prasankumar, R. P.; Upadhya, P. C.; Taylor, A. J. Ultrafast Carrier Dynamics in Semiconductor Nanowires. *Phys. Stat. Sol. B* **2009**, *246*, 1973–1995.
6. Johnson, J.; Knutsen, K.; Yan, H.; Law, M.; Zhang, Y.; Yang, P.; Saykally, R. Ultrafast Carrier Dynamics in Single ZnO Nanowire and Nanoribbon Lasers. *Nano Lett.* **2004**, *4*, 197–204.
7. Song, J. K.; Willer, U.; Szarko, J. M.; Leone, S. R.; Li, S.; Zhao, Y. Ultrafast Upconversion Probing of Lasing Dynamics in Single ZnO Nanowire Lasers. *J. Phys. Chem. C* **2008**, *112*, 1679–1684.
8. Robel, I.; Bunker, B. A.; Kamat, P. V.; Kuno, M. Exciton Recombination Dynamics in CdSe Nanowires: Bimolecular to Three-Carrier Auger Kinetics. *Nano Lett.* **2006**, *6*, 1344–1349.
9. Puthussery, J.; Lan, A.; Kosel, T. H.; Kuno, M. Band-filling of Solution-Synthesized CdS Nanowires. *ACS Nano* **2008**, *2*, 357–367.
10. Carey, C. R.; Yu, Y.; Kuno, M.; Hartland, G. V. Ultrafast Transient Absorption Measurements of Charge Carrier Dynamics in Single II–VI Nanowires. *J. Phys. Chem. C* **2009**, *113*, 19077–19081.
11. Glennon, J. J.; Buhro, W. E.; Loomis, R. A. Simple Surface-Trap-Filling Model for Photoluminescence Blinking Spanning Entire CdSe Quantum Wires. *J. Phys. Chem. C* **2008**, *112*, 4813–4817.
12. Vietmeyer, F.; Frantsuzov, P. A.; Janko, B.; Kuno, M. Carrier Recombination Dynamics in Individual CdSe Nanowires. *Phys. Rev. B* **2011**, *83*, 115319.
13. Schmitt-Rink, S.; Miller, D.; Chemla, D. Theory of the Linear and Nonlinear Optical-Properties of Semiconductor Microcrystallites. *Phys. Rev. B* **1987**, *35*, 8113–8125.
14. Gammon, D.; Snow, E.; Shanabrook, B.; Katzer, D.; Park, D. Homogeneous Linewidths in the Optical Spectrum of a Single Gallium Arsenide Quantum Dot. *Science* **1996**, *273*, 87–90.
15. Takagahara, T. Theory of Exciton Dephasing in Semiconductor Quantum Dots. *Phys. Rev. B* **1999**, *60*, 2638–2652.
16. Shah, J.; *Ultrafast Spectroscopy of Semiconductors and Semiconductor Nanostructures*, 2nd ed.; Springer: Germany, 1999.
17. Vaurette, F.; Leturcq, R.; Nys, J. P.; Deresmes, D.; Grandidier, B.; Stievenard, D. Evidence of Electron-Phonon Interaction on Transport in n- and p-type Silicon Nanowires. *Appl. Phys. Lett.* **2008**, *92*, 242109.
18. Liptay, T.; Marshall, L.; Rao, P.; Ram, R.; Bawendi, M. Anomalous Stokes Shift in CdSe Nanocrystals. *Phys. Rev. B* **2007**, *76*, 155314.
19. Saviot, L.; Champagnon, B.; Duval, E.; Kudriavtsev, I. A.; Ekimov, A. I. Size Dependence of Acoustic and Optical Vibrational Modes of CdSe Nanocrystals in Glasses. *J. Non-Cryst. Solids* **1996**, *197*, 238–246.
20. Woggon, U.; Gindele, F.; Wind, O.; Klingshim, C. Exchange Interaction and Phonon Confinement in CdSe Quantum Dots. *Phys. Rev. B* **1996**, *54*, 1506–1509.
21. Saviot, L.; Champagnon, B.; Duval, E.; Ekimov, A. I. Size-Selective Resonant Raman Scattering in CdS Doped Glasses. *Phys. Rev. B* **1998**, *57*, 341–346.
22. Fernee, M. J.; Littleton, B. N.; Cooper, S.; Rubinsztein-Dunlop, H.; Gomez, D. E.; Mulvaney, P. Acoustic Phonon Contributions to the Emission Spectrum of Single CdSe Nanocrystals. *J. Phys. Chem. C* **2008**, *112*, 1878–1884.
23. Krauss, T.; Wise, F. Coherent Acoustic Phonons in a Semiconductor Quantum Dot. *Phys. Rev. Lett.* **1997**, *79*, 5102–5105.
24. Son, D. H.; Wittenberg, J. S.; Banin, U.; Alivisatos, A. P. Second Harmonic Generation and Confined Acoustic Phonons in Highly Excited Semiconductor Nanocrystals. *J. Phys. Chem. B* **2006**, *110*, 19884–19890.
25. Sagar, D. M.; Cooney, R. R.; Sewall, S. L.; Kambhampati, P. State-Resolved Exciton–Phonon Couplings in CdSe Semiconductor Quantum Dots. *J. Phys. Chem. C* **2008**, *112*, 9124–9127.
26. Huxter, V. M.; Lee, A.; Lo, S. S.; Scholes, G. D. CdSe Nanoparticle Elasticity and Surface Energy. *Nano Lett.* **2009**, *9*, 405–409.
27. McKimmie, L. J.; Lincoln, C. N.; Jasieniak, J.; Smith, T. A. Three-Pulse Photon Echo Peak Shift Measurements of Capped CdSe Quantum Dots. *J. Phys. Chem. C* **2010**, *114*, 82–88.
28. Tyagi, P.; Cooney, R. R.; Sewall, S. L.; Sagar, D. M.; Saari, J. I.; Kambhampati, P. Controlling Piezoelectric Response in Semiconductor Quantum Dots *via* Impulsive Charge Localization. *Nano Lett.* **2010**, *10*, 3062–3067.
29. Hartland, G. V. Optical Studies of Dynamics in Noble Metal Nanostructures. *Chem. Rev.* **2011**, *111*, 3858–3887.
30. Klimov, V. I. Optical Nonlinearities and Ultrafast Carrier Dynamics in Semiconductor Nanocrystals. *J. Phys. Chem. B* **2000**, *104*, 6112–6123.
31. Kambhampati, P. Unraveling the Structure and Dynamics of Excitons in Semiconductor Quantum Dots. *Acc. Chem. Res.* **2011**, *44*, 1–13.
32. Yan, Y.; Chen, G.; Van Patten, P. G. Ultrafast Exciton Dynamics in CdTe Nanocrystals and Core/Shell CdTe/CdS Nanocrystals. *J. Phys. Chem. C* **2011**, *115*, 22717–22728.
33. Klimov, V. I.; McBranch, D. W.; Leatherdale, C. A.; Bawendi, M. G. Electron and Hole Relaxation Pathways in Semiconductor Quantum Dots. *Phys. Rev. B.* **1999**, *60*, 13740.
34. Guyot-Sionnest, P.; Wehrenberg, B.; Yu, D. Intraband Relaxation in CdSe Nanocrystals and the Strong Influence of the Surface Ligands. *J. Chem. Phys.* **2005**, *123*, 074709.
35. Sewall, S.; Cooney, R.; Anderson, K.; Dias, E.; Kambhampati, P. State-to-State Exciton Dynamics in Semiconductor Quantum Dots. *Phys. Rev. B* **2006**, *74*, 235328.
36. Knowles, K. E.; McArthur, E. A.; Weiss, E. A. A Multi-timescale Map of Radiative and Nonradiative Decay Pathways for Excitons in CdSe Quantum Dots. *ACS Nano* **2011**, *5*, 2026–2035.
37. Zhu, H.; Song, N.; Rodriguez-Cordoba, W.; Lian, T. Q. Wave Function Engineering for Efficient Extraction of up to Nineteen Electrons from One CdSe/CdS Quasi-Type II Quantum Dot. *J. Am. Chem. Soc.* **2012**, *134*, 4250–4257.

38. Kuno, M.; Ahmad, O.; Protasenko, V.; Bacinello, D.; Kosel, T. H. Solution-Based Straight and Branched CdTe Nanowires. *Chem. Mater.* **2006**, *18*, 5722–5732.
39. Arbouet, A.; Christofilos, D.; Del Fatti, N.; Vallee, F.; Huntzinger, J. R.; Arnaud, L.; Billaud, P.; Broyer, M. Direct Measurement of the Single-Metal-Cluster Optical Absorption. *Phys. Rev. Lett.* **2004**, *93*, 127401.
40. Celebrano, M.; Kukura, P.; Renn, A.; Sandoghdar, V. Single-Molecule Imaging by Optical Absorption. *Nat. Photon.* **2011**, *5*, 95–98.
41. Carey, C. R.; LeBel, T.; Crisostomo, D.; Giblin, J.; Kuno, M.; Hartland, G. V. Imaging and Absolute Extinction Cross-Section Measurements of Nanorods and Nanowires through Polarization Modulation Microscopy. *J. Phys. Chem. C* **2010**, *114*, 16029–16036.
42. Ruppin, R. Extinction by a Circular Cylinder in an Absorbing Medium. *Opt. Commun.* **2002**, *211*, 335–340.
43. Glennon, J. J.; Tang, R.; Buhro, W. E.; Loomis, R. A.; Bussian, D. A.; Htoon, H.; Klimov, V. I. Exciton Localization and Migration in Individual CdSe Quantum Wires at Low Temperatures. *Phys. Rev. B* **2009**, *80*, 081303.
44. Schafer, S.; Wang, Z.; Zierold, R.; Kipp, T.; Mews, A. Laser-Induced Charge Separation in CdSe Nanowires. *Nano Lett.* **2011**, *11*, 2672–2677.
45. Rode, D. L. Electron Mobility in II−VI Semiconductors. *Phys. Rev. B* **1970**, *2*, 4036–4044.
46. Rudin, S.; Reinecke, T. L.; Segall, B. Temperature-Dependent Exciton Linewidths in Semiconductors. *Phys. Rev. B* **1990**, *42*, 11218–11231; *Phys. Rev. B* **1995**, *52*, 11517.
47. Pandey, A.; Guyot-Sionnest, P. Hot Electron Extraction from Colloidal Quantum Dots. *J. Phys. Chem. Lett.* **2010**, *1*, 45–47.
48. Sewall, S. L.; Cooney, R. R.; Anderson, K. E. H.; Dias, E. A.; Sagar, D. M.; Kambhampati, P. State-Resolved Studies of Biexcitons and Surface Trapping Dynamics in Semiconductor Quantum Dots. *J. Chem. Phys.* **2008**, *129*, 084701.
49. Mortimer, R. G. *Mathematics for Physical Chemistry*, 2nd ed.; Academic Press: San Diego, CA, 1999.
50. Mehl, B. P.; Kirschbrown, J. R.; House, R. L.; Papanikolas, J. M. The End is Different than the Middle: Spatially Dependent Dynamics in ZnO Rods Observed by Femtosecond Pump-Probe Microscopy. *J. Phys. Chem. Letters* **2011**, *2*, 1777–1781.
51. Burda, C.; Link, S.; Mohamed, M.; El-Sayed, M. A. The Pump Power Dependence of the Femtosecond Relaxation of CdSe Nanoparticles Observed in the Spectral Range from Visible to Infrared. *J. Chem. Phys.* **2002**, *116*, 3828–3833.
52. Klingshirn, C. F. *Semiconductor Optics*, 3rd ed; Springer: New York, 2007.
53. Galland, C.; Ghosh, Y.; Steinbrück, A.; Sykora, M.; Hollingsworth, J. A.; Klimov, V. I.; Htoon, H. Two Types of Luminescence Blinking Revealed by Spectro-Electrochemistry of Single Quantum Dots. *Nature* **2011**, *479*, 203.
54. Hu, M.; Wang, X.; Hartland, G. V.; Mulvaney, P.; Juste, J.; Sader, J. Vibrational Response of Nanorods to Ultrafast Laser Induced Heating: Theoretical and Experimental Analysis. *J. Am. Chem. Soc.* **2003**, *125*, 14925–14933.
55. Simmons, G.; Wang, H. *Single Crystal Elastic Constant and Calculated Aggregate Properties: A Handbook*, 2nd ed.; The M.I.T. Press: Cambridge, MA, 1971.
56. Nelet, A.; Crut, A.; Arbouet, A.; Del Fatti, N.; Vallee, F.; Portales, H.; Saviot, L.; Duval, E. Acoustic Vibrations of Metal Nanoparticles: High Order Radial Mode Detection. *Appl. Surf. Sci.* **2004**, *226*, 209–215.
57. Yadav, H. K.; Gupta, V.; Sreenivas, K.; Singh, S. P.; Sundarakannan, B.; Katiyar, R. S. Low Frequency Raman Scattering from Acoustic Phonons Confined in ZnO Nanoparticles. *Phys. Rev. Lett.* **2006**, *97*, 085502.
58. Duval, E.; Boukenter, A.; Champagnon, B. Vibration Eigenmodes and Size of Microcrystallites in Glass—Observation by Very-Low-Frequency Raman-Scattering. *Phys. Rev. Lett.* **1986**, *56*, 2052–2055.
59. Staleva, H.; Skrabalak, S. E.; Carey, C. R.; Kosel, T.; Xia, Y.; Hartland, G. V. Coupling to Light, and Transport and Dissipation of Energy in Silver Nanowires. *Phys. Chem. Chem. Phys.* **2009**, *11*, 5889–5896.
60. Tchebotareva, A. L.; Ruijgrok, P. V.; Zijlstra, P.; Orrit, M. Probing the Acoustic Vibrations of Single Metal Nanoparticles by Ultrashort Laser Pulses. *Laser Photon. Rev.* **2010**, *4*, 581–597.
61. Pelton, M.; Sader, J. E.; Burgin, J.; Liu, M. Z.; Guyot-Sionnest, P.; Gosztola, D. Damping of Acoustic Vibrations in Gold Nanoparticles. *Nat. Nanotechnol.* **2009**, *4*, 492–495.
62. Dubrovskiy, V. A.; Morochnik, V. S. Natural Vibrations of a Spherical Inhomogeneoity in an Elastic Medium. *Earth Phys.* **1981**, *17*, 494–504.
63. Voisin, C.; Del Fatti, N.; Christofilos, D.; Vallee, F. Time-Resolved Investigation of the Vibrational Dynamics of Metal Nanoparticles. *Appl. Surf. Sci.* **2000**, *164*, 131–139.
64. Burgin, J.; Langot, P.; Del Fatti, N.; Vallee, F.; Huang, W.; El-Sayed, M. A. Time-Resolved Investigation of the Acoustic Vibration of a Single Gold Nanoprism Pair. *J. Phys. Chem. C* **2008**, *112*, 11231–11235.
65. Marty, R.; Arbouet, A.; Girard, C.; Mlayah, A.; Paillard, V.; Lin, V. K.; Teo, S. L.; Tripathy, S. Damping of the Acoustic Vibrations of Individual Gold Nanoparticles. *Nano Lett.* **2011**, *11*, 3301–3306.
66. Saviot, L.; Netting, C. H.; Murray, D. B. Damping by Bulk and Shear Viscosity of Confined Acoustic Phonons for Nanostructures in Aqueous Solution. *J. Phys. Chem. B* **2007**, *111*, 7457–7461.
67. Ruijgrok, P. V.; Zijlstra, P.; Tchebotareva, A. L.; Orrit, M. Damping of Acoustic Vibrations of Single Gold Nanoparticles Optically Trapped in Water. *Nano Lett.* **2012**, *12*, 1063–1069.
68. Trentler, T. J.; Goel, S. C.; Hickman, K. M.; Viano, A. M.; Chiang, M. Y.; Beatty, A. M.; Gibbons, P. C.; Buhro, W. E. Solution−Liquid−Solid Growth of Indium Phosphide Fibers from Organometallic Precursors: Elucidation of Molecular and Nonmolecular Components of the Pathway. *J. Am. Chem. Soc.* **1997**, *119*, 2172–2181.
69. Yan, Y.; Wang, L.; Vaughn, C. B.; Chen, G.; Van Patten, P. G. Spectroscopic Investigation of Oxygen Sensitivity in CdTe and CdTe/CdS Nanocrystals. *J. Phys. Chem. C* **2011**, *115*, 24521–24527.